Specifications and Design of a PM Electric Variable Transmission for Toyota Prius II

Yuan Cheng, Rochdi Trigui, *Member, IEEE*, Christophe Espanet, *Member, IEEE*, Alain Bouscayrol, *Member, IEEE*, and Shumei Cui

***Abstract*—This paper focuses on an analysis of technical requirements for the design of a permanent-magnet-type electric variable transmission (PM-EVT), which is a novel series–parallel hybrid electric vehicle (HEV) powertrain concept. Similar to the planetary gear train used in Toyota Prius II, the EVT also realizes the power-split function. However, it is implemented in an electromagnetic way rather than in a mechanical way, as is the case for Prius II with a planetary gear. In this paper, a procedure to define the technical requirements of an EVT is presented. Since Toyota Prius II is a well-known series–parallel HEV, this vehicle is chosen as a reference. The engine, battery, and other necessary components are kept as input data. A dynamic simulation was performed to take into account different driving cycles. Then, based on an analysis of the simulation results (torque, speed, and power) the technical requirements of the PM-EVT are defined. Finally, the PM-EVT machine is designed. The PM-EVT design results are presented and validated using the finite-element method (FEM).**

***Index Terms*—Electric variable transmission (EVT), permanent-magnet machine, planetary gear, series–parallel hybrid electric vehicle (HEV).**

I. Introduction

DUE TO THE pressure of environmental pollution and the current energy crisis, hybrid electric vehicles (HEVs) have gained increasing attention. With regard to different architectures, HEVs fall into three categories, namely, series hybrid, parallel hybrid, and series–parallel hybrid. Despite having more complex structures, series–parallel HEVs (SP-HEVs) combine the advantages of both series and parallel hybrids and have greater potential in improving fuel economy and reducing emissions [1]–[4]. As a well-known SP-HEV, Toyota Prius II uses a planetary gear to optimize power flows.

Various SP-HEV topologies can be found [5]–[7]. Among them, the concept of an electric variable transmission (EVT) also realizes the series–parallel function. However, it is implemented in an electromagnetic way rather than in a mechanical way, as is the case with Toyota Prius II. In the EVT, a combination of two concentrically arranged electric machines is adopted. By controlling their speed and torque, an integrated powertrain function is enabled, including a continuously variable transmission, a starter, and a generator [8]–[10].

Different machine types and structures can be applied to such a powertrain concept, and several studies have been carried out, with areas of focus including machine performance improvement and its applications in HEVs [11]–[24]. In a previous study [25], a permanent-magnet EVT (PM-EVT) was chosen because of its higher efficiency and torque density [26], [27]. Different PM-EVT structures have been analyzed, as well as a step-by-step choice of an appropriate structure for EVTs.

Thus, SP-HEVs can be developed using a planetary gear train or an EVT. To obtain an efficient comparison, both solutions have to be studied in the framework of the same vehicle for the same use. Since the first steps, however, the design of HEVs has been carried out as a whole, including the choice of the powertrain [28], [29]. In our approach, we propose to design an EVT for an existent HEV with a planetary gear train. Second, the EVT could be integrated into the global model of the vehicle to replace the planetary gear. Finally, comparative studies could be carried out examining efficiency, performance, and limitations. The design of an EVT for an existing vehicle, however, is not an easy task. This subsystem has to ensure the same functionalities as the planetary gear train solution. The technical requirements of the HEV have to be analyzed first. The EVT then has to be designed in accordance with these technical requirements.

The objective of this paper is to design an EVT which fulfills the requirements of Toyota Prius II. The next step is to integrate this EVT into the same simulation model of the vehicle for comparative purposes. As Toyota Prius II is a well-known SP-HEV with a real vehicle available in our group, this HEV has been chosen as the reference vehicle.

This paper is organized as follows: In Section II, the Prius and EVT-HEV systems will be briefly introduced with respect to their structures, principles, etc. In Section III, the Prius simulation is first carried out using the software VEHLIB to obtain the technical data for defining the EVT specifications. Extracting the simulation data, the maximum and rated specifications

Manuscript received November 15, 2010; revised February 20, 2011; accepted April 20, 2011. Date of publication May 19, 2011; date of current version December 9, 2011. This work was supported by "Nord-Pas-de-Calais," France and was performed within the Modélisation Énergétique et Gestion d'Énergie des Véhicules Hybrides: the French network on hybrid electric vehicles. The review of this paper was coordinated by Dr. A. Davoudi.

Y. Cheng is with the Institute of Electromagnetic and Electronic Technology, Harbin Institute of Technology, Harbin 150001, China, and also with the Laboratory of Electrotechnics and Power Electronics, University of Lille 1, 59655 Villeneuve d'Ascq, France (e-mail: chengyuan@hit.edu.cn).

R. Trigui is with the Transport and Environment Laboratory, French Institute of Science and Technology for Transport, Development and Networks, 69675 Bron, France (e-mail: rochdi.trigui@ifsttar.fr).

C. Espanet is with the Institut Franche-Comté Électronique, Mécanique, Thermique et Optique-Sciences et Technologies, Energie et Ingénierie des Systèmes Multiphysiques, University of Franche-Comte, 90010 Belfort, France (e-mail: christophe.espanet@univ-fcomte.fr).

A. Bouscayrol is with the Laboratory of Electrotechnics and Power Electronics, University of Lille 1, 59655 Villeneuve d'Ascq, France (e-mail: Alain.Bouscayrol@univ-lille1.fr).

S. Cui is with the Institute of Electromagnetic and Electronic Technology, Harbin Institute of Technology, Harbin 150001, China (e-mail: cuism@hit.edu.cn).

Color versions of one or more of the figures in this paper are available online at http://ieeexplore.ieee.org.

Digital Object Identifier 10.1109/TVT.2011.2155106

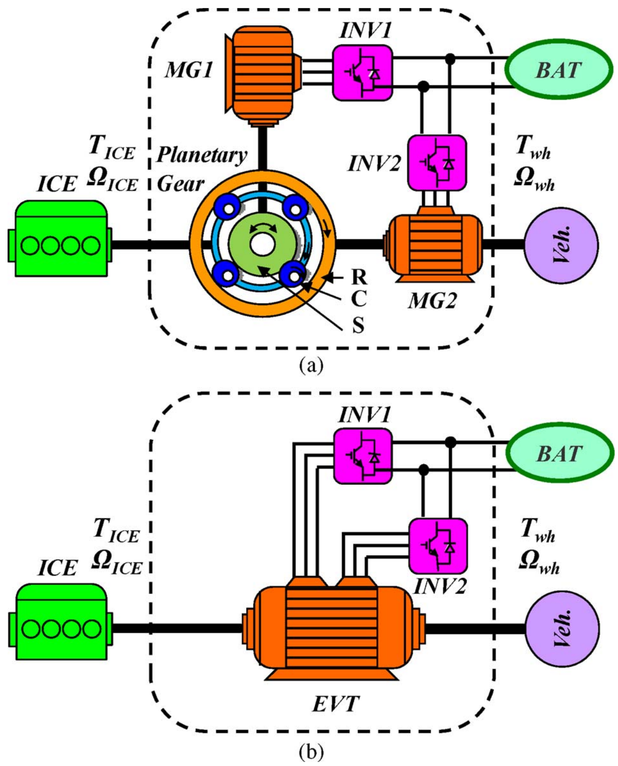

Fig. 1. Two SP-HEV powertrains. (a) Toyota Prius II system. (b) EVT system.

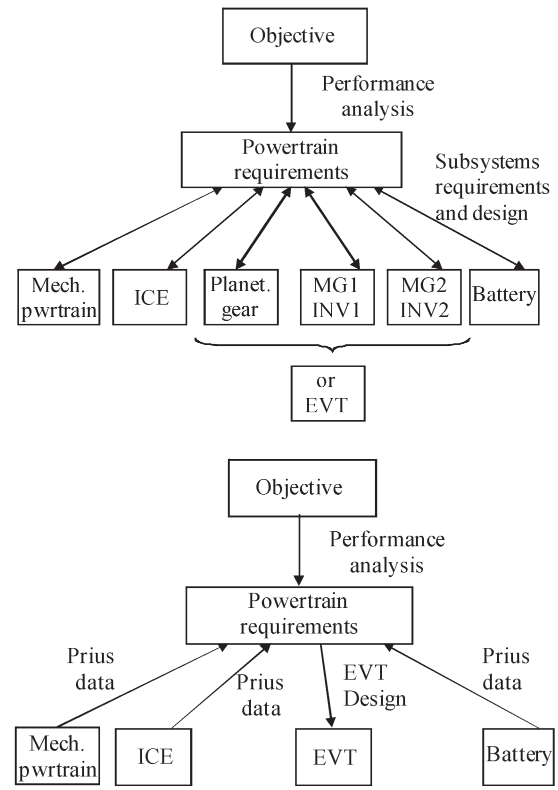

Fig. 2. EVT design procedure.

are defined. In Section IV, to illustrate the interest of the defined specifications, an initial PM-EVT is designed using a proposed design procedure. The main analytical design equations are given, and the finite-element method (FEM) results are used to validate the design.

II. Series-Parallel Hybrid Electric Vehicle Powertrains

The SP-HEV allows a power-split operation in both series and parallel hybrid paths and creates more freedom to optimize the power flows. The power-split function can be implemented in different ways. To design an EVT system, a system-level design procedure is also presented based on an analysis of the operation of Prius II (see Fig. 2).

A. SP-HEV With a Planetary Gearbox

In Prius II, the planetary gear (PG) is used to connect different power plants. The PG consists of a set of gears, namely, the ring gear (R), the sun gear (S), and the carrier gear (C). As shown in Fig. 1(a), the internal combustion engine (ICE) is linked to the carrier. Electric motor/generator 1 (MG1) is connected to the sun gear, whereas MG2 is connected to the ring gear and then to the vehicle, which enables direct motor propulsion and energy recycling into the battery (BAT) during regenerative braking [31]–[35].

B. SP-HEV With a PM-EVT

In this case, the electrical machines are denoted EM1 and EM2 to clearly distinguish them from the electrical machines in the planetary gear solution. An EVT is another device that realizes the power-split function in an electromechanical way rather than in a mechanical way. In principle, the EVT is considered as an integrated electromechanical converter consisting of two concentrically arranged electric machines (EM1 + EM2). Two sets of three phase windings are fed by two power converters (INV1 and INV2) with a common dc bus, as shown in Fig. 1(b).

C. EVT Design Procedure

Due to the nature of the SP-HEV, the series–parallel powertrain design is more complex than that of a conventional automobile and the series or parallel HEVs. It must be designed at a system level. All power subsystems are co-designed to obtain the technical requirements of the powertrain. In the case of an EVT, this new device replaces MG1, MG2 and the planetary gear. The EVT generally is co-designed with other subsystems.

In our case, however, the final objective is to compare an EVT solution with the Prius II solution. This is why the actual engine, the mechanical powertrain, and the battery subsystem of Prius II are left unchanged. Their characteristics will be used as input data for the EVT design in the proposed design procedure (see Fig. 2). Vehicle performances, driving cycles, and energy management will be the same as for Prius II in this first study.

III. Technical Requirements for Permanent-Magnet-Type Electric Variable Transmission

To obtain the technical requirements for the PM-EVT, Prius II is simulated according to different performance requirements and a developed control strategy. The simulation results are extracted and applied into the studied EVT-HEV to analyze and define the specifications of the EVT.

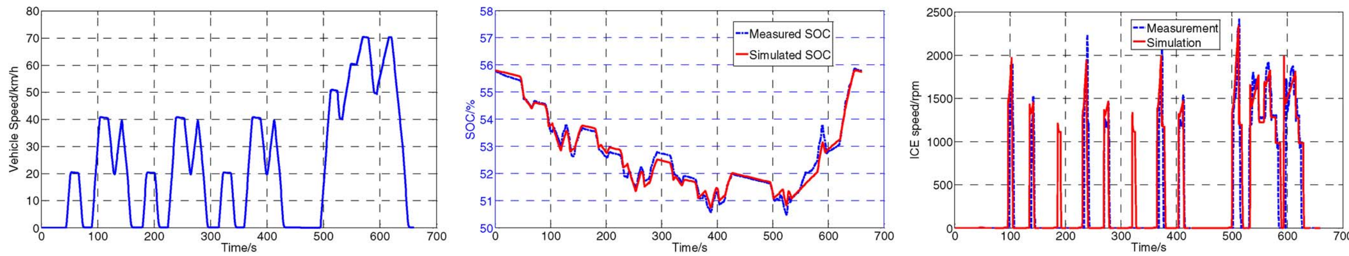

(a) (b) (c)

Fig. 3. VEHLIB validation by experiments based on the 1015 cycle [36]. (a) Vehicle speed in the 1015 cycle. (b) Battery SOC. (c) ICE speed.

TABLE I
SIMULATION PARAMETERS OF TOYOTA PRIUS II

Vehicle weight/kg	1360	Battery energy/kWh	1.3
Rolling radius/m	0.3	Battery voltage/V	201.6
Frontal area/m^2	1.746	Final drive ratio	4.113
Rolling resistance	0.0054	ICE engine/kW	57
Air friction coeff.	0.26	Planetary gear	2.6(78/30)

A. Prius Simulation

The Prius system is simulated using VEHLIB software based on the MATLAB/Simulink environment [36], [37]. In VEHLIB software, modeling the vehicle consists of modeling its different units (ICE, electric machines, batteries, gears, etc.) and their interactions by means of a strict forward-looking approach. A simulation of Toyota Prius II has been developed using VEHLIB. A real Prius vehicle has been used to validate this simulation model using experimental results, both on different components and on the whole vehicle. Fig. 3 shows a comparison of simulation and measurement results, with some significant variables based on the 1015 driving cycle (state of charge (SOC) of the battery, vehicle speed, and ICE speed). The 1015 driving cycle is an abbreviation of the Japanese-mode 1015 driving cycle, which reflects the typical driving environment in Japan. It has been chosen because the studied Toyota Prius was imported from Japan (designed for Japanese users).

More validation results can be found in [36], including dynamic performance tests under different SOCs of the battery. Due to the use of the energy management for EV mode, some differences occur, as explained in [36]. The other results, however, indicate good correlation between measurement and simulation. Therefore, the VEHLIB simulation for Prius can be considered accurate enough to be used in what follows.

Taking into account various performance requirements, the following driving cycles are simulated:

1) maximum acceleration performance of 0–180 km/h in 100 s;
2) highway cycle with a maximum speed of 140 km/h and an average speed of 92 km/h;
3) road cycle with a maximum speed of 104 km/h and an average speed of 48 km/h;
4) urban cycle with a maximum speed of 58 km/h and an average speed of 22 km/h.

Moreover, another acceleration performance test is also considered, which occurs on a 5% slope. However, the simulation results show that its performance requirement could be covered by the maximum acceleration performance. Therefore, the acceleration on a slope will not be included in this paper. Some parameters of Toyota Prius II are listed in Table I [36].

B. Analysis of Technical Requirements

For the analysis of the technical requirements, a detailed EVT structure is illustrated in Fig. 4. The EVT can be considered as an integrated electromechanical converter consisting of two concentrically arranged electric machines. Outer machine EM2 consists of an external stator and the outer part of an outer rotor. Inner machine EM1 consists of an inner rotor and the inner part of an outer rotor. Two layers of surface-mounted permanent magnets (SMPM) are attached on the outer rotor.

Dynamic models of two SP-HEVs using the planetary gear and the EVT are presented. More details about modeling the PG and the EVT are given in [5], [6], [10], and [34]–[38].

In Prius II, the speeds and torques of ICE, MG1, and MG2, i.e., $\Omega_{\mathrm{ICE}}, \Omega_{\mathrm{MG1}}, \Omega_{\mathrm{MG2}}$ and $T_{\mathrm{ICE}}, T_{\mathrm{MG1}}, T_{\mathrm{MG2}}$, respectively, satisfy the relationship, as defined in (1). ρ is known as the basic ratio, which is equal to $78/30 = 2.6$. In a steady state, the torque dynamics reduces to (2). Similarly, for the EVT-HEV, the equations of dynamics are described in (3), as well as the steady-state equations in (4). $\Omega_{\mathrm{EM1}}, \Omega_{\mathrm{EM2}}$ and $T_{\mathrm{EM1}}, T_{\mathrm{EM2}}$ are the speeds and electromagnetic torques of EM1 and EM2, respectively. F_{res} is the resistance force, which includes the rolling resistance and the aerodynamic resistance. r_w and k_t are the radius of the wheel and the final drive ratio in the Prius II case, respectively. J_{EVT1} and J_{EVT2} are the equivalent inertia values on the input and output shafts of the EVT. J_{PG1}, J_{PG2}, J_{PG3}, and J_{PG4} are the equivalent inertia values of Prius II. The aforementioned equations are given as follows:

$$
\begin{aligned}
&\text{Speed}: \begin{cases} \Omega_{\mathrm{ICE}} = \frac{\rho}{1+\rho} \cdot \Omega_{\mathrm{MG2}} + \frac{1}{1+\rho} \cdot \Omega_{\mathrm{MG1}} \\ \Omega_{\mathrm{MG2}} = \frac{k_t}{r_w} \cdot v_{\mathrm{veh}} \end{cases} \\
&\text{Torque}: \begin{cases} J_{\mathrm{PG1}} \frac{d\Omega_{\mathrm{ICE}}}{dt} = T_{\mathrm{ICE}} - (\rho+1) T_{\mathrm{MG1}} \\ \qquad\qquad - J_{\mathrm{PG2}} \frac{d\Omega_{\mathrm{MG2}}}{dt} \\ J_{\mathrm{PG3}} \frac{d\Omega_{\mathrm{MG2}}}{dt} = T_{\mathrm{MG2}} + \frac{\rho}{\rho+1} T_{\mathrm{ICE}} - T_{\mathrm{res}} \\ \qquad\qquad + J_{\mathrm{PG4}} \frac{d\Omega_{\mathrm{ICE}}}{dt} \\ T_{\mathrm{res}} = \frac{r_w}{k_t} F_{\mathrm{res}} \end{cases}
\end{aligned} \tag{1}
$$

$$
\text{Torque}: \begin{cases} T_{\mathrm{MG1}} = \frac{1}{\rho+1} T_{\mathrm{ICE}} \\ T_{\mathrm{res}} = T_{\mathrm{MG2}} + \frac{\rho}{\rho+1} T_{\mathrm{ICE}} \end{cases} \tag{2}
$$

$$
\begin{aligned}
&\text{Speed}: \begin{cases} \Omega_{\mathrm{ICE}} = \Omega_{\mathrm{EM2}} - \Omega_{\mathrm{EM1}} \\ \Omega_{\mathrm{EM2}} = \frac{k_t}{r_w} \cdot v_{\mathrm{veh}} \end{cases} \\
&\text{Torque}: \begin{cases} J_{\mathrm{EVT1}} \frac{d\Omega_{\mathrm{ICE}}}{dt} = T_{\mathrm{ICE}} - T_{\mathrm{EM1}} \\ J_{\mathrm{EVT2}} \frac{d\Omega_{\mathrm{EM2}}}{dt} = T_{\mathrm{EM2}} + T_{\mathrm{EM1}} - T_{\mathrm{res}} \\ T_{\mathrm{res}} = \frac{r_w}{k_t} F_{\mathrm{res}} \end{cases}
\end{aligned} \tag{3}
$$

$$
\text{Torque}: \begin{cases} T_{\mathrm{ICE}} = T_{\mathrm{EM1}} \\ T_{\mathrm{res}} = T_{\mathrm{EM2}} + T_{\mathrm{EM1}}. \end{cases} \tag{4}
$$

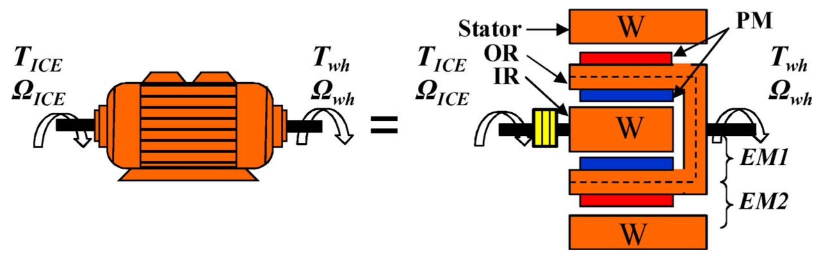

Fig. 4. SMPM-EVT structure.

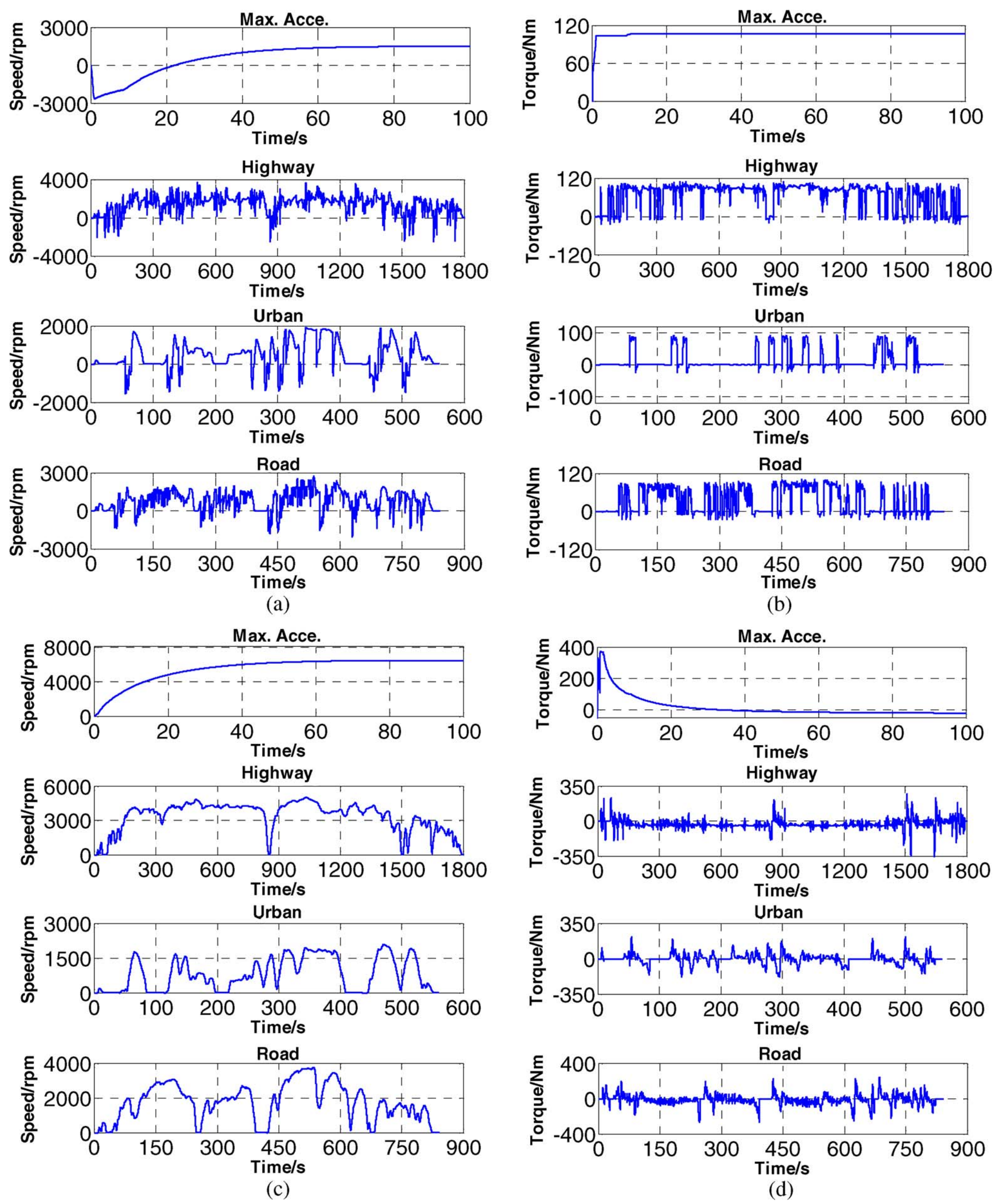

Fig. 5. EVT speed and torque curves deduced from Prius II simulation. (a) EM1 speed. (b) EM1 torque. (c) EM2 speed. (d) EM2 torque.

Using the dynamic and steady models, the torque and speed curves under different driving cycles are obtained (see Fig. 5). The distribution of the operation points in the torque–speed plan is thus shown in Fig. 6.

EM1 aims to transmit ICE torque T_{ICE} to the vehicle and to realize a change of speed between the ICE and the vehicle requirement. The output shaft of EM2 is mechanically linked to the final drive so that its speed is proportional to the vehicle speed. EM2 needs to compensate the torque difference between the ICE and the vehicle requirements.

Based on the foregoing understanding of the missions of the EVT, working areas for EM1 and EM2 can be defined by four

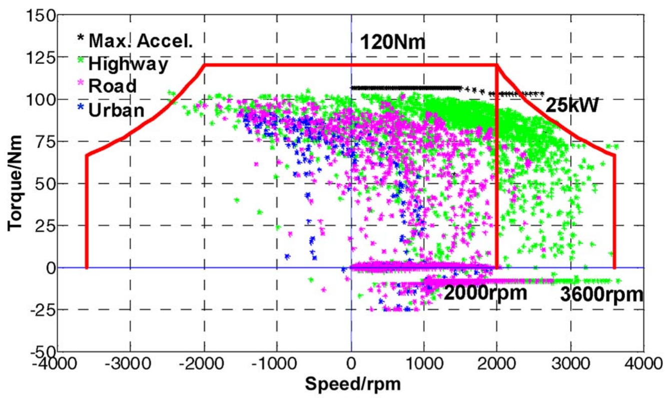

(a)

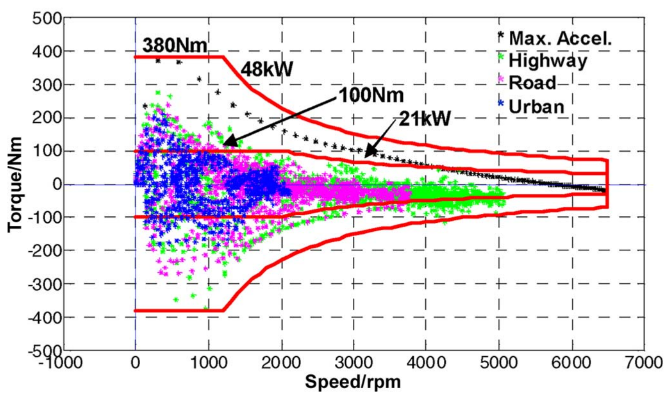

(b)

Fig. 6. EVT operation points in the torque–speed plan. (a) EM1 torque–speed distribution. (b) EM2 torque–speed distribution.

parameters, namely, maximum and rated torques and maximum and rated speeds. The choices of these parameters are analyzed as follows.

1) Maximum Speeds and Torques for EM1 and EM2: For EM1, its torque output has to cover the whole ICE working range to deliver its torque to the vehicle. Considering the dynamics, its maximum torque $T_{\mathrm{EM1\_max}}$ should be a little higher than the real ICE torque.

Defining the maximum speed of EM1, i.e., $\Omega_{\mathrm{EM1\_max}}$, is more complex because Ω_{EM1} depends on the difference between Ω_{ICE} and Ω_{EM2}. Although the maximum vehicle speed is defined, the choice of Ω_{ICE} is difficult due to its optimized operation. Due to the proposed design procedure in Section II, $\Omega_{\mathrm{EM1\_max}}$ can be estimated on the basis of simulation of different driving cycles. As shown in Fig. 6(a), because the vehicle speed is higher in the highway cycle than in the urban and road cycles, Ω_{EM1} is also higher. In the maximum acceleration test, although the vehicle speed is greater, Ω_{ICE} is also greater, reaching nearly 5000 r/min. Therefore, $\Omega_{\mathrm{EM1\_max}}$ occurs in the highway cycle, which is equal to 3600 r/min.

EM2 is mechanically connected to the final drive. Its maximum speed $\Omega_{\mathrm{EM2\_max}}$ is proportional to the maximum vehicle speed of 180 km/h, which is equal to 6500 r/min.

As for MG2 in Prius II, EM2 must provide enough short-term torque $T_{\mathrm{EM2\_max}}$ to satisfy the acceleration performance requirements. Meanwhile, during regenerative braking, EM2 is also necessary to have the short-term overload capability to recover the braking energy.

As shown in Fig. 6(b), the maximum torque of EM2, i.e., $T_{\mathrm{EM2\_max}}$, is a little lower than that of MG2 ($T_{\mathrm{MG2\_max}} = 400\ \mathrm{N \cdot m}$). Indeed, in Toyota Prius, the ICE is mechanically linked to MG2 via the planetary gear. From (1) and (2), it can be seen that the ICE torque contributes to the total traction torque in the ratio of $\rho/(1+\rho)$. Comparatively, in the EVT-HEV, the ICE torque contributes to the final drive, as defined in (3) and (4). Therefore, EM2 needs a lower torque to satisfy the same performance requirements.

2) Rated Speeds and Torques for EM1 and EM2: During highway cruising, EM1 has to transmit the ICE torque, mainly ranging from 80 to 100 $\mathrm{N \cdot m}$, in the long term. Moreover, to achieve the maximum acceleration capability, EM1 must deliver the maximum ICE torque for a duration of 100 s. Therefore, rated torque $T_{\mathrm{EM1\_rat}}$ is chosen equal to $T_{\mathrm{EM1\_max}}$.

Unlike electric machines working around the rated region, the EV electric machines have to work in a wide torque–speed range (see Fig. 6). Therefore, generally, its rated speed and torque are not easily obtained. In this paper, statistical distributions based on Fig. 6 are used to define the rated speeds and torques for EM1 and EM2. Fig. 7 shows the distribution of speeds, torques, and power values of EM1 and EM2 for the given intervals. The cumulative percentage distribution, which gives the sum of all the percentages of occurrences, is also calculated for each parameter.

The EM1 rated speed $\Omega_{\mathrm{EM1\_rat}}$ of 2000 r/min is finally adopted, which covers 92% of the speed operation points. Field weakening is an important factor in choosing this value to achieve a reasonable extended speed range.

In addition, the rated torque of EM2, i.e., $T_{\mathrm{EM2\_rat}}$, is statistically estimated. Since the thermal limit has to be satisfied to avoid ruining the machines, a reasonable overload ratio needs to be chosen. Finally, $T_{\mathrm{EM2\_}rat}$ is chosen as 100 $\mathrm{N \cdot m}$, which covers nearly 95% of the operating points, as shown in Fig. 7.

Rated power $P_{\mathrm{EM2\_rat}}$ is chosen, which covers 95% of the operating points. $P_{\mathrm{EM2\_rat}}$ corresponds to rated speed $\Omega_{\mathrm{EM2\_rat}}$, which is equal to 2000 r/min. It is a reasonable value when considering the field-weakening operation during high speeds.

Finally, the rated and maximum specifications of the EVT are listed in Table II, along with those of the Prius machines, for comparative purposes. As shown in Fig. 6, a few operation points are beyond the defined torque–speed range of EVT machines. However, its ratio to the overall operation points is very small and is thus neglected.

IV. Design and Validation of the Permanent-Magnet-Type Electric Variable Transmission

An initial PM-EVT has been designed to fulfill the aforementioned analytical results. Independent design is first adopted without considering the magnetic interference between EM1 and EM2. The effect of magnetic interference will be discussed later.

To design the PM-EVT, the main design equations for a normal PMSM, as given in [39] and [40], are recalled here. The overall dimensions of an electric machine are defined according to its electromagnetic torque, i.e.,

$$T = 2\pi r^2 l B_{1g} K_{1s} \tag{5}$$

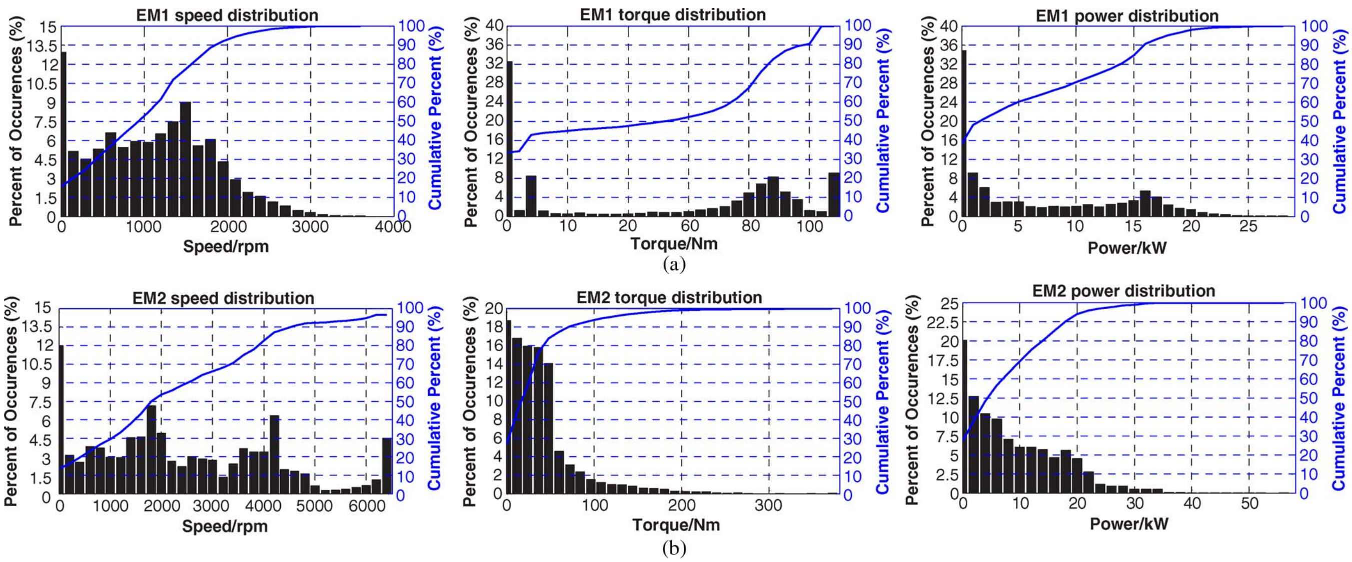

Fig. 7. Statistical distributions of EVTs. (a) Statistical distributions for EM1. (b) Statistical distributions for EM2.

TABLE II
SPECIFICATIONS OF EVT AND PRIUS ELECTRIC MACHINES

	EVT			
	EM1		EM2	
	T/Nm	*P/kW*	*T/Nm*	*P/kW*
Rated values	120@ 0~2krpm	25@ 2k~3.6krpm	100@ 0~2krpm	21@ 2k~6.5krpm
Max. values	120@ 0~2krpm	25@ 2k~3.6krpm	380@ 0~1.2krpm	48@ 1.2k~6.5krpm
	Prius			
	MG1		**MG2**	
	T/Nm	*P/kW*	*T/Nm*	*P/kW*
Max. values	160@ 0~1.8krpm	30@ 1.8krpm	400@ 0~1.2krpm	50@ 1.2krpm

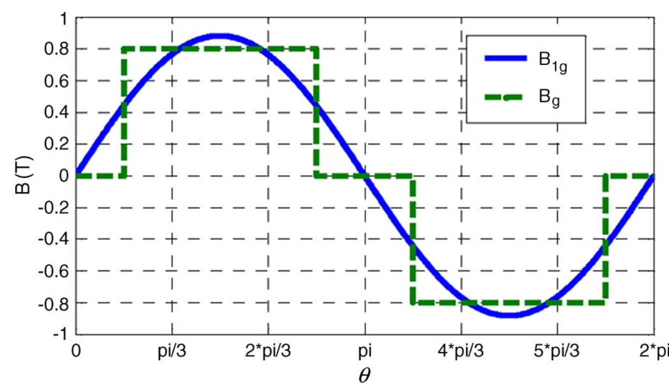

Fig. 8. Air-gap flux density waveform.

where r is the rotor radius, l is the rotor length, B_{1g} is the root-mean-square value of the fundamental sinusoidal space component of the air-gap flux density created by the magnet, and K_{1s} is the linear current density along the stator periphery. B_{1g} and K_{1s} are limited by many design constraints, including the magnet properties, geometric dimensions, saturation, and cooling capability [39], [40].

Air-gap flux density is assumed to have the waveform presented in Fig. 8. The relationship between B_{1g} and air-gap flux density magnitude B_g is thus given by

$$B_{1g} = \frac{2\sqrt{2}}{\pi} B_g \sin(\alpha) \tag{6}$$

where α is the electrical angle of the magnet span ranging from 55° to 80°. B_g is in the range of 0.85–0.95 T.

The following empirical equation is used to calculate minimum air gap g_m above the magnets:

$$g_m \approx 0.0002 + 0.003\sqrt{r \cdot l}, \quad g_e = 1.05 g_m. \tag{7}$$

Moreover, an arbitrary 5% increase of g_m is assumed to calculate effective air gap g_e taking the effect of Carters' coefficient into account.

Thus, radial thickness l_m of the permanent magnet is defined by

$$l_m = \frac{\mu_r g_e}{B_r / B_g - 1} \tag{8}$$

where μ_r and B_r are the relative permeability and the residual flux density, respectively. For the NdFeB magnet, $\mu_r \approx 1.05$ and $B_r \approx 1.1$ T. When ignoring the flux leakages, one half of the flux in every magnet goes through the yoke. Therefore, the yoke thickness can be expressed as

$$d_y = \frac{\alpha \cdot r}{p_n} \cdot \frac{B_g}{B_y} \tag{9}$$

where p_n is the number of pole pairs, and B_y is the maximum yoke flux density, which is constrained by the core saturation. Typically, B_y is in the range of 1.4–1.7 T, varying to adjust to the core losses.

More details about the PM-EVT design can be found in [25], including the design of slots and windings and the number of turns. The final geometry of the PM-EVT is shown in Fig. 9, as well as the no-load flux lines using the FEM. The main

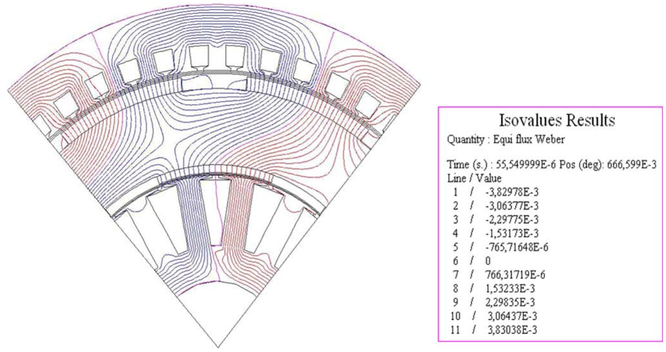

Fig. 9. No-load flux lines of the PM-EVT under the rated speed.

TABLE III
MAIN PARAMETERS OF PM-EVT AND PRIUS MG2

Parameters	EM1	EM2	MG2-Prius
Number of poles	6	8	8
Inner rotor outer radius/mm	80	--	56.3
Outer rotor inner radius/mm	86	--	--
Outer rotor outer radius/mm	--	122	--
Stator inner radius/mm	--	130	81.2
Stator outer radius/mm	--	160	133.6
Machine length/mm	160	160	83.6
Air gap length/mm	1.5	2	2
Thickness of magnets/mm	4.5	6	--
Magnet span (α)/°	120	120	--
Number of slots per pole per phase	1	2	2
Rated voltage/V	220	220	--
Resistance per phase/mΩ	115.4	118.9	--
Inductances (L_d=L_q)/mH	2.683	0.654	--
PM flux linkage/Wb	0.53	0.401	--
Specific power/kW/kg	0.92	0.99	1.11

parameters of the PM-EVT are listed in Table III, as well as those of Prius MG2, for comparative purposes [32], [33]. Due to the fact that MG1 data could not be obtained, only MG2 data are listed.

From the EVT flux lines, it can be seen that magnetic interference exists between EM1 and EM2, which will affect the machine performance. In [25], it has been proven that the interference changes with the relative position angle $\Delta\beta$ of the outer and inner magnets in the PM-EVT. Since the reduction of the flux densities in the air gaps is less than 2%, it has been concluded that the effect of magnetic interference on the EVT performance can be ignored with sufficient accuracy for an initial approach.

The validation of the machine performance was carried out based on FEM simulation. Since the two machines adopt the same design equations with a few differences, only EM2 is taken as an example to validate the design.

Fig. 10(a) shows the back electromotive force (EMF) results using the analytical method and FEM simulation under the rated speed. A comparison of the fundamental components of the back EMF has indicated good agreement. Due to the stator slotting and the rotor flux leakage, the back EMF using an analytical method is 4.7% higher than the FEM result, which is in a reasonable range.

The FEM torque simulation is also given in comparison with the design value, as shown in Fig. 10(b). A torque reduction

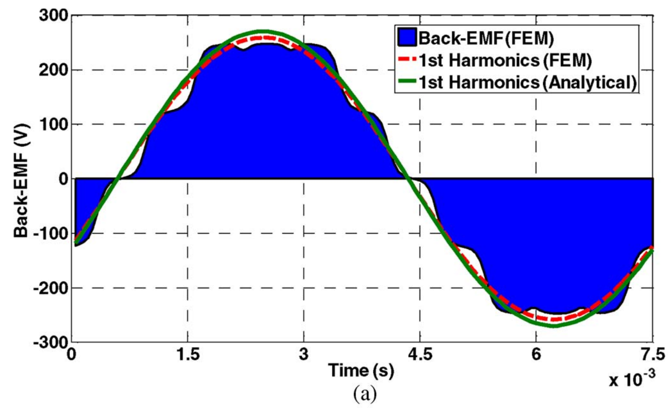

(a)

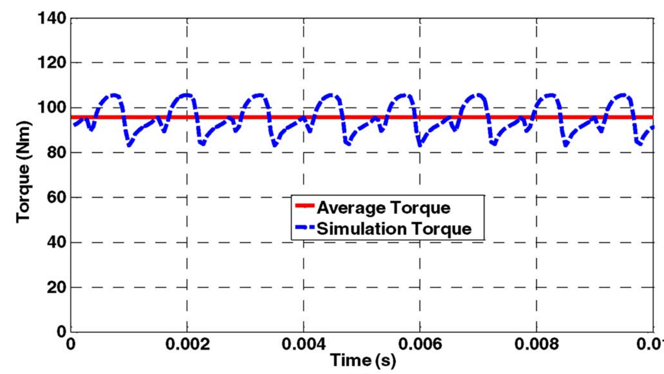

(b)

Fig. 10. Comparison of FEM and analytical results. (a) Back EMF and its fundamental component. (b) Torque simulation and analytical results.

of 4.2% is within reasonable limits considering the reduction of air-gap flux density due to the stator slotting and leakage. The field-weakening and overload capabilities are also validated using the FEM. Although the air-gap flux is distorted due to the armature reaction during the overload operation, the simulated maximum torque of EM2 still meets the design requirements.

An initial comparison of the PM-EVT and Prius II machines can be undertaken (EM2 and MG2 in fact). The volume of EM2 is greater than that of MG2. This is because the EVT is an integrated electromechanical converter, in which EM1 is inserted into EM2. Therefore, only specific power is compared. As listed in Table III, the EM2 specific power is almost equal to 1 kW/kg, in comparison with that of 1.11 kW/kg for the MG2 in Prius II. Since the designed EVT is an initial attempt, no machine optimization has been carried out. This explains the performance differences. On the other hand, EM2 adopts a surface-mounted PM machine, and MG2 is an interior PM-type machine. The later machine exhibits a reluctance torque in addition to the magnetic torque, which also helps increase the power density [33].

Deducing from a common model and control structure, it has been proven that the EVT-HEV and Toyota Prius II have the same basic power flows and operation modes [41], [42]. Using the same methodology, a comparison of the performance and efficiency is being developed. However, since the objective of this paper is to define the technical specifications of the EVT-HEV, such a comparison is beyond the content of this paper. It will be developed in future work.

V. Conclusion and Future Work

A new SP-HEV has been developed. It is composed of an EVT, instead of electrical machines, and a planetary gear. A PM-EVT has been designed for Toyota Prius II to replace the current powertrain using a planetary gear. This way, future comparisons could be developed to highlight the advantages and drawbacks of both solutions.

Toyota Prius II has been chosen as the reference vehicle because it is a well-known and efficient system. We have proposed a new design procedure, which begins with finding the technical requirements of the EVT, where the ICE, mechanical powertrain, and supply subsystems are used as input data. The simulation of Prius II provided various results, and the obtained evolution of torques and speeds was used to complete the requirements of the EVT. A specific PM-EVT was then designed, and a finite-element simulation validated its ability to meet the technical requirements. Although the proposed design method is developed for the particular case of Toyota Prius II and an initial design of the PM-EVT, it could still be considered for the design and analysis of other hybrid powertrains. Thus, it can be considered as a generic method to define the specifications of hybrid powertrains.

The next steps of this work are given here.

1) Machine optimization will be carried out to improve the performance of the PM-EVT, including specific power and thermal modeling.
2) Global modeling and control of both the EVT-HEV and Prius II will then be detailed for a more in-depth comparison, particularly in terms of dynamic and energetic behaviors.

References

[1] C. C. Chan, “The state of the art of electric, hybrid and fuel cell vehicles,” *Proc. IEEE*, vol. 95, no. 4, pp. 704–718, Apr. 2007.

[2] C. C. Chan, A. Bouscayrol, and K. Chen, “Electric, hybrid, and fuel-cell vehicles: Architectures and modeling,” *IEEE Trans. Veh. Technol.*, vol. 59, no. 2, pp. 589–598, Feb. 2010.

[3] M. Ehsani, Y. Gao, S. E. Gay, and A. Emadi, *Modern Electric, Hybrid Electric, and Fuel Cell Vehicles: Fundamentals, Theory, and Design*. Boca Raton, FL: CRC, Dec. 2004.

[4] A. Emadi, K. Rajashekara, S. S. Williamson, and S. M. Lukic, “Topological overview of hybrid electric and fuel cell vehicular power systems architectures and configurations,” *IEEE Trans. Veh. Technol.*, vol. 54, no. 3, pp. 763–770, May 2005.

[5] J. M. Miller, “Hybrid electric vehicle propulsion system architectures of the e-CVT type,” *IEEE Trans. Power Electron.*, vol. 21, no. 3, pp. 756–767, May 2006.

[6] J. M. Miller and M. Everett, “An assessment of ultracapacitors as the power cache in Toyota THS-II, GM-Allison AHS-2 and Ford FHS hybrid propulsion systems,” in *Proc. IEEE APEC*, 2005, pp. 481–490.

[7] B. Mashadi and S. A. M. Emadi, “Dual-mode power-split transmission for hybrid electric vehicles,” *IEEE Trans. Veh. Technol.*, vol. 59, no. 7, pp. 3223–3232, Sep. 2010.

[8] M. J. Hoeijmakers and J. A. Ferreira, “The electric variable transmission,” *IEEE Trans. Ind. Appl.*, vol. 42, no. 4, pp. 1092–1093, Jul./Aug. 2006.

[9] M. J. Hoeijmakers and M. Rondel, “The electrical variable transmission in a city bus,” in *Proc. 35th IEEE PESC*, Aachen, Germany, 2004, pp. 2773–2778.

[10] Y. Cheng, S. Cui, L. Song, and C. C. Chan, “The study of the operation modes and control strategies of an advanced electromechanical converter for automobiles,” *IEEE Trans. Magn.*, vol. 43, no. 1, pp. 430–433, Jan. 2007.

[11] Y. Cheng, K. Chen, C. C. Chan, A. Bouscayrol, and S. Cui, “Global modeling and control strategy simulation for a hybrid electric vehicle using electrical variable transmission,” *IEEE Veh. Technol. Mag.*, vol. 4, no. 2, pp. 73–79, Jun. 2009.

[12] E. Nordlund and C. Sadarangani, “The four quadrant energy transducer,” in *Conf. Rec. 37th IEEE IAS Annu. Meeting*, 2002, pp. 390–391.

[13] L. Xu, “A new breed of electric machines—Basic analysis and applications of dual mechanical port electric machines,” in *Proc. 8th Int. Conf. Elect. Mach. Syst.*, 2005, pp. 24–29.

[14] P. Zheng, R. Liu, Q. Wu, J. Zhao, and Z. Yao, “Magnetic coupling analysis of four-quadrant transducer used for hybrid electric vehicles,” *IEEE Trans. Magn.*, vol. 43, no. 6, pp. 2597–2599, Jun. 2007.

[15] X. Guo, T. Fan, X. Wen, and F. Zhao, “Electromagnetic coupling analysis of uniform magnetic-filed permanent magnet dual mechanical port machine,” in *Proc. 11th ICEMS*, Wuhan, China, 2008, pp. 3181–3184.

[16] J. T. B. A. Kessels, D. L. Foster, and P. P. J. van den Bosch, “Integrated powertrain control for hybrid electric vehicles with electric variable transmission,” in *Proc. IEEE VPPC*, Sep. 2009, pp. 376–381.

[17] M. Aubertin, A. Tounzi, and Y. L. Menach, “Study of an electromagnetic gearbox involving two permanent magnet synchronous machines using 3-D-FEM,” *IEEE Trans. Magn.*, vol. 44, no. 11, pp. 4381–4384, Nov. 2008.

[18] Y. Gao and M. Ehsani, “A torque and speed coupling hybrid drive–train–architecture, control, and simulation,” *IEEE Trans. Power Electron.*, vol. 21, no. 3, pp. 741–748, May 2006.

[19] Y. Cheng, “Research on hybrid powertrain based on four ports electromechanical converter,” Ph.D. dissertation, Harbin Inst. Technol., Harbin, China, Apr., 2009.

[20] Y. J. Yuan, “Research on switched reluctance four port electromechanical energy transducer used for wind power,” M.S. thesis, Harbin Inst. Technol., Harbin, China, Jun., 2008.

[21] S. Cui, L. Song, S. Han, Y. Cheng, and C. C. Chan, “Switched reluctance machine based electromechanical converter with four ports,” Chinese invention patent, Application No. 200710072358.5, Jun. 15, 2007.

[22] Y. B. Wang, M. Cheng, Y. Fan, and K. T. Chau, “A double-stator permanent magnet brushless machine system for electric vehicle transmission in hybrid electric vehicles,” in *Proc. IEEE VPPC*, 2010, pp. 1–5.

[23] F. G. Zhang, G. W. Liu, Y. S. Shen, and F. X. Wang, “Characteristic study on a novel PMSM with opposite-rotation dual rotors,” in *Proc. 10th ICEMS*, Seoul, Korea, 2007, pp. 805–809.

[24] R. Liu, P. Zheng, H. Zhao, and C. Sadarangani, “Investigation of a compound-structure permanent-magnet synchronous machine used for HEVs,” in *Proc. IEEE VPPC*, Sep. 2008, pp. 1–5.

[25] Y. Cheng, C. Espanet, R. Trigui, A. Bouscayrol, and S. Cui, “Design of a permanent magnet electric variable transmission for HEV applications,” in *Proc. IEEE VPPC*, 2010, pp. 1–5.

[26] Z. Q. Zhu, “Electrical machines and drives for electric, hybrid and fuel cell vehicles,” *Proc. IEEE*, vol. 95, no. 4, pp. 746–765, Apr. 2007.

[27] K. T. Chau, C. C. Chan, and C. Liu, “Overview of permanent-magnet brushless drives for electric and hybrid electric vehicles,” *IEEE Trans. Ind. Electron.*, vol. 55, no. 6, pp. 2246–2257, Jun. 2008.

[28] M. Ehsani, K. M. Rahman, and H. A. Toliyat, “Propulsion system design of electric and hybrid vehicles,” *IEEE Trans. Ind. Electron.*, vol. 44, no. 1, pp. 19–27, Feb. 1997.

[29] A. H. Niasar, H. Moghbelli, and A. Vahedi, “Design methodology of drive train for a series–parallel hybrid electric vehicle (SP-HEV) and its power flow control strategy,” in *Proc. Int. Conf. Elect. Mach. Drives*, 2005, pp. 1549–1554.

[30] X. Guo, X. Wen, F. Zhao, and T. Fan, “Power parameters matching design of dual mechanical ports electric machine with clutch applied in hybrid electric vehicle,” in *Proc. ICEMS*, 2008, pp. 3595–3599.

[31] S. Sasaki, “Toyota’s newly developed hybrid powertrain,” in *Proc. ISPSD*, Kyoto, Japan, Jun. 1998, pp. 17–22.

[32] R. H. Staunton, C. W. Ayers, L. D. Marlino, J. N. Chiasson, and T. A. Burress, “Evaluation of 2004 Toyota Prius hybrid electric drive system,” Univ. Tennessee-Knoxville, Oak Ridge Inst. Sci. Educ., Oak Ridge, TN, ORNL/TM-2006/423, May 2006.

[33] J. S. Hsu, C. W. Ayers, and C. L. Coomer, “Report on Toyota/Prius motor design and manufacturing assessment,” UT-Battelle, LLC, Oak Ridge Nat. Lab., Oak Ridge, TN, ORNL/TM-2004/137, Aug. 2004.

[34] K. Chen, A. Bouscayrol, A. Berthon, P. Delarue, D. Hissel, and R. Trigui, “Global modeling of different vehicles, using energetic macroscopic representation to focus on system function and system energy properties,” *IEEE Veh. Technol. Mag.*, vol. 4, no. 2, pp. 80–89, Jun. 2009.

[35] J. Lin and H. Peng, “Modeling and control of a power-split hybrid vehicle,” *IEEE Trans. Control Syst. Technol.*, vol. 16, no. 6, pp. 1242–1251, Nov. 2008.

[36] E. Vinot, J. Scordia, R. Trigui, B. Jeanneret, and F. Badin, “Model simulation, validation and case study of the 2004 THS of Toyota Prius,” *Int. J. Vehicle Syst. Model. Test.*, vol. 3, no. 3, pp. 139–167, 2008.

[37] K. Chen, R. Trigui, A. Bouscayrol, E. Vinot, W. Lhomme, and A. Berthon, "A common model validation in the case of the Toyota Prius II," in *Proc. IEEE VPPC*, 2010, pp. 1–5.
[38] F. U. Syed, M. L. Kuang, J. Czubay, and H. Ying, "Derivation and experimental validation of a power-split hybrid electric vehicle model," *IEEE Trans. Veh. Technol.*, vol. 55, no. 6, pp. 1731–1747, Nov. 2006.
[39] G. R. Slemon and X. Liu, "Modelling and design optimization of permanent magnet motors," *Elect. Mach. Power Syst.*, vol. 20, no. 2, pp. 71–92, Mar./Apr. 1992.
[40] G. R. Slemon, "On the design of high-performance surface-mounted PM motors," *IEEE Trans. Ind. Appl.*, vol. 30, no. 1, pp. 134–140, Jan./Feb. 1994.
[41] K. Chen, W. Lhomme, A. Bouscayrol, and A. Berthon, "Comparison of two series–parallel hybrid electric vehicles focusing on control structures and operation modes," in *Proc. IEEE VPPC*, 2009, pp. 1–8.
[42] K. Chen, "Common energetic macroscopic representation and unified control structure for different hybrid electric vehicles," Ph.D. dissertation, Univ. Lille 1, Lille, France, May, 2010.

Yuan Cheng received the B.S., M.Sc., and Ph.D. degrees from Harbin Institute of Technology (HIT), Harbin, China, in 2002, 2004, and 2009, respectively, all in electrical engineering.

In 2006, he joined the Department of Electrical Engineering, HIT. He is currently a Postdoctoral Researcher with the Laboratory of Electrotechnics and Power Electronics, University of Lille 1, Villeneuve d'Ascq, France, in the frame of Modélisation Énergétique et Gestion d'Énergie des Véhicules Hybrides network. His research interests include electric machine drives and control, modeling, and control of electric and hybrid vehicles.

Rochdi Trigui (M'06) was born in Sfax, Tunisia, in 1969. He received the electrical engineering degree from the National High School of Electrical and Mechanical Engineering, Nancy, France, in 1993 and the Ph.D. degree in electrical engineering from the National Polytechnic Institute of Lorraine, Nancy, in 1997.

Since 1998, he has been a Researcher in the field of electric and hybrid vehicles with the French National Institute for Transport and Safety Research (INRETS), Bron, France. Since 2008, he has been the head of the Hybrid Electric Vehicle team with INRETS, now called the French Institute of Science and Technology for Transport, Development and Networks (IFST-TAR). He is an Associate Editor of the *Journal of Asian Electric Vehicle*.

Dr. Trigui is currently a member of the French network Modélisation Énergétique et Gestion d'Énergie des Véhicules Hybrides for hybrid vehicle modeling and control and of the IEEE Vehicular Technology Society. He was the Cochair of the IEEE Vehicle Power and Propulsion Conference in 2010.

Christophe Espanet (M'04) received the Laurea degree from "Ecole Normale Supérieure," Paris, France, and the Ph.D. degree from the University of Franche-Comte, Belfort, France, in 1999. His Ph.D. thesis dealt with the design and optimization of permanent-magnet (PM) high-torque in-wheel motors.

From 1999 to 2007, he was an Associate Professor with the Laboratory of Electrical Engineering and Systems, Belfort, France. He is currently a Full Professor with the University of Franche-Comte and Head of the Energy Conversion Systems Design Research Team with the Institut Franche-Comté Électronique, Mécanique, Thermique et Optique-Sciences et Technologies. His research interests include the modeling and design of electrical systems, particularly PM synchronous machines.

Alain Bouscayrol (M'02) received the Ph.D. degree in electrical engineering from the National Polytechnic Institute of Toulouse, Toulouse, France, in 1995.

He was an Associate Professor with the Laboratory of Electrotechnics and Power Electronics, University of Lille 1, Villeneuve d'Ascq, France, in 1996 and later became a Professor in 2005. From 1998 to 2004, he managed the "Multimachine Muticonverter Systems" project of the National Research Group SDSE-ME2MS of the French National Scientific Research Centre. Since 2005, he has been managing Modélisation Énergétique et Gestion d'Énergie des Véhicules Hybrides, which is a French national network on hybrid vehicles. His research interests include graphical descriptions for electrical machine control, traction applications, and hybrid vehicles.

Shumei Cui received the B.S., M.S., and Ph.D. degrees from Harbin Institute of Technology (HIT), Harbin, China, in 1987, 1990, and 1998, respectively, all in electrical engineering.

Since 2001, she has been a Professor with the Department of Electrical Engineering, HIT. She is currently the Vice Dean of the Institute of Electromagnetic and Electronic Technology, HIT, and the Dean of the Electric Vehicle Research Centre. Her research interests focus on the design and control of micro and special electric machines, electric drive systems of electric vehicles, control and simulation of hybrid electric vehicles, and intelligent test and fault diagnostics of electric machines.